



26 measurements of all the parameters involved in the theoretical calculation of the observed  
27  $O_2(b^1\Sigma_g^+ - X^3\Sigma_g^-)(0,0)$  emission, i.e. temperature and density of the background air, atomic  
28 oxygen density, and volume emission rate, is the novelty and the advantage of this work.

29

## 30 **1. Introduction**

31

32 The mesopause region is essential to understand the chemical and physical processes in the  
33 upper atmosphere because this is region of coldest temperature (during summer at high  
34 latitudes) and highest turbulence in the atmosphere (e.g. Lübken, 1997), the region of  
35 formation of such phenomena as NLC and PMSE (e.g. Rapp and Lübken, 2004), the region of  
36 gravity waves (GWs) breaking and formation of secondary GWs (Becker and Vadas, 2018),  
37 as well as the region of coupling between mesosphere and thermosphere. This region is  
38 characterised by different airglow emissions and, particularly, by the emissions of the  
39 Atmospheric Band which is produced by the excited state of molecular oxygen  $O_2(b^1\Sigma_g^+)$ .  
40 Airglow observation in the Atmospheric Band is a useful method to study dynamical  
41 processes in the mesopause region. There have been a number of reports of gravity waves  
42 (GWs) detection in this band (Noxon, 1978; Viereck and Deehr, 1989; Zhang et al., 1993).  
43 Planetary wave climatology has been investigated by the Spectral Airglow Temperature  
44 Imager (SATI) instrument (Lopez-Gonzalez et al., 2009). In addition, the parameters of tides  
45 have been reported from SATI (Lopez-Gonzalez et al., 2005) and High Resolution Doppler  
46 Imager (HRDI) observations (Marsh et al., 1999). In number of works Sheese et al. (2010,  
47 2011) inferred the temperature by Atmospheric Band observation. Furthermore, the response  
48 of mesopause temperature and atomic oxygen during major sudden stratospheric warming  
49 was studied utilising Atmospheric Band emission by Shepherd et al. (2010). Various works  
50 have focused on Atmospheric Band emission modelling with respect to gravity waves and  
51 tides (e.g. Hickey et al., 1993; Leko et al., 2002; Liu and Swenson, 2003). The specific theory

52 of the gravity wave effects on  $O_2(b^1\Sigma_g^+)$  emission was derived in Tarasick and Shepherd  
53 (1992). Moreover, Atmospheric Band observations have been widely utilised to infer atomic  
54 oxygen, which is an essential chemical constituent for energetic balance in the extended  
55 mesopause region (e.g. Hedin et al., 2009, and references there in), and ozone concentration  
56 (Mlynczak et al., 2001). Although there is a large field of application of Atmospheric Band  
57 emissions, there is a lack of knowledge on processes of the  $O_2(b^1\Sigma_g^+)$  population. Two main  
58 mechanisms of night-time population (note, the day-time mechanisms are quite different, see  
59 e.g. Zarboon et al., (2018)) were proposed: the first is the direct population from three-body  
60 recombination of atomic oxygen (e. g. Deans et al., 1976); the second is the so-called two-  
61 step mechanism, which assumes an intermediate excited precursor  $O_2^*$  (e. g. Witt et al., 1984;  
62 Greer et al., 1981). It has been shown by laboratory experiments that the first mechanism  
63 alone has not explained observed emissions (Young and Sharpless, 1963; Clyne et al., 1965;  
64 Young and Black, 1966; Bates, 1988). The second mechanism entails a discussion about the  
65 precursor excited state and additional ambiguities in their parameters (e.g. Greer et al., 1981;  
66 Ogryzlo et al., 1984). Thus, Witt et al. (1984) proposed the hypothesis that the  $O_2(c^1\Sigma_u^-)$  state  
67 is, possibly, the precursor; López-González et al. (1992a) suppose that the precursor could be  
68  $O_2(^5\Pi_g)$ ; Wildt et al. (1991) found by laboratory measurements that it could be  $O_2(A^3\Sigma_u^+)$ .  
69 Hence, the problem of identification is still not solved. The essential step in this direction has  
70 been done after the ETON 2 (Energy Transfer in the Oxygen Nightglow) rocket experiment.  
71 ETON 2 mission yielded empirical fitting parameters that allow either to quantify the  
72  $O_2(b^1\Sigma_g^+)$  (and, consequently, volume emission) by known O, or atomic oxygen by known  
73 volume emission values (McDade et al., 1986). Despite the significance of this work, the  
74 temperature and density of air (necessary for derivation) were taken from CIRA-72 and  
75 MSIS-83 (Hedin, 1983) models. This leads to some degree of uncertainty (e.g. Murtagh et al.,  
76 1990). Thus, more solid knowledge on these fitting coefficients based on consistent

77 measurements of atomic oxygen, volume emission of Atmospheric Band, and temperature  
78 and density of background atmosphere is desirable. In this paper we present common volume  
79 measurements of these parameters performed in the course of WADIS-2 sounding rocket  
80 mission. In the next section, we describe the rocket experiment and obtained data relevant for  
81 our study. In section 3, to make the paper easier to understand, we repeat some theoretical  
82 approximations from McDade et al. (1986). The obtained results of our calculations are  
83 discussed in section 4. Concluding remarks and summary are given in the last section.

84

## 85 **2. Rocket experiment Description**

86

87 The WADIS (Wave propagation and dissipation in the middle atmosphere: Energy budget and  
88 distribution of trace constituents) sounding rocket mission aimed to simultaneously study the  
89 propagation and dissipation of GWs and measure the concentration of atomic oxygen. It  
90 comprised two field campaigns conducted at the Andøya Space Center (ASC) in northern  
91 Norway (69°N, 16°E). The WADIS-2 sounding rocket was launched during the second  
92 campaign on 5 March 2015 at 01:44:00 UTC, that is, night-time conditions. For a more  
93 detailed mission description, the reader is referred to Strelnikov et al. (2017) and the  
94 accompanying paper by Strelnikov et al. (2018).

95 The WADIS-2 sounding rocket was equipped with the CONE instrument to measure absolute  
96 neutral air density and temperature with high spatial resolution, instrument for atomic oxygen  
97 density measurements FIPEX (Flux Probe Experiment) and the Airglow Photometer for  
98 atmospheric band (762 nm) volume emission observation.

99 CONE (COMbined measurement of Neutrals and Electrons), operated by IAP (Leibniz  
100 Institute of Atmospheric Physics at the Rostock University), is a classical triode type  
101 ionisation gauge optimised for a pressure range between  $10^{-5}$  to 1 mbar. The triode system is  
102 surrounded by two electrodes: Whilst the outermost grid is biased to +3 to +6 V to measure

103 electron densities at a high spatial resolution, the next inner grid (-15 V) is meant to shield the  
104 ionisation gauge from ionospheric plasma. CONE is suitable for measuring absolute neutral  
105 air number densities at altitude range between 70 and 120 km. To obtain absolute densities,  
106 the gauges are calibrated in the laboratory using a high-quality pressure sensor, like a  
107 Baratron. The measured density profile can be further converted to a temperature profile  
108 assuming hydrostatic equilibrium. For a detailed description of the CONE instrument, see  
109 Giebeler et al. (1993) and Strelnikov et al. (2013). Molecular oxygen and molecular nitrogen  
110 are derived from CONE atmospheric number density measurements and partitioning  
111 according to NRLMSISE-00 reference atmosphere (Picone et al., 2002).

112 The Airglow Photometer operated by MISU (Stockholm University, Department of  
113 Meteorology) measures the emission of the molecular oxygen Atmospheric Band around 762  
114 nm from the overhead column, from which volume emission rate is inferred by  
115 differentiation. For airglow measurements in general, a filter photometer is positioned under  
116 the nose cone viewing along the rocket axis with a defined field-of-view (FOV). For WADIS-  
117 2 however, the FOV of  $\pm 3^\circ$  was tilted from the rocket axis by  $3^\circ$  to avoid having other parts of  
118 the payload within the FOV and at the same time roughly view the same volume as the other  
119 instruments. The optical design is a standard radiometer-type system with an objective lens, a  
120 field lens, aperture and stops which provide an even illumination over a large portion of the  
121 detector surface (photomultiplier tube) and a defined FOV. At the entrance of the photometer  
122 there is an interference filter with a passband of 6 nm centred at 762 nm. During ascent, after  
123 the nosecone ejection, the photometer then counts the incoming photons from the overhead  
124 column (or actually the overhead cone). When the rocket passes through the layer the  
125 measured photon flux drops and above the emission layer only weak background emissions  
126 are present (e.g. the zodiacal and galactic light). After the profile has been corrected for  
127 background emissions and attitude (van Rhijn effect) it is converted from counts to radiance  
128 using pre-flight laboratory calibrations. The calibration considers the spectral shape of the 0-0

129 band of the  $O_2(b^1\Sigma_g^+ - X^3\Sigma_g^-)(0,0)$  Atmospheric Band system and the overlap of the  
130 interference filter passband. The profile is then smoothed and numerically differentiated with  
131 respect to altitude to yield the volume emission rate of the emitting layer. The data were  
132 sampled with 1085 Hz which results in an altitude resolution of about 0.75 m during the  
133 passage of the airglow layer (the velocity was  $\sim 800$  m/s at 95 km). However, because of the  
134 high noise level, the profile needed to be averaged to a vertical resolution of at least 3 km in  
135 order to get satisfactory results after the differentiation. A more detailed description and  
136 review of this measurement technique is given by Hedin et al. (2009).

137 The aim of the FIPEX developed by the IRS (Institute of Space Systems, University of  
138 Stuttgart) is to measure the atomic oxygen density along the rocket trajectory with high spatial  
139 resolution. It employs solid electrolyte sensor which has a selective sensitivity to atomic  
140 oxygen. A low voltage is applied between anode and cathode pumping oxygen ions through  
141 the electrolyte ceramic (yttria stabilised zirconia). The current measured is proportional to the  
142 oxygen density. Sampling is realised with a frequency of 100 Hz and enables a spatial  
143 resolution of  $\sim 10$  m. Laboratory calibrations were done for molecular and atomic oxygen. For  
144 a detailed description of the FIPEX instruments and their calibration techniques see Eberhart  
145 et al. (2015, 2018).

146

### 147 **3. Theory**

148

149 Here, we are repeating the theory of  $O_2(b^1\Sigma_g^+ - X^3\Sigma_g^-)(0,0)$  night-time emissions following  
150 McDade et al. (1986) to make our paper more readable, using all nomenclature as in the  
151 original paper. All utilised reactions are listed in Table 1, together with corresponding  
152 reaction rates, branching ratios, quenching rates and spontaneous emission coefficients. Some  
153 components have been updated according to modern knowledge, thus, deviating from the  
154 work of McDade et al. (1986).

155 Assuming direct one-step mechanism as a main one for population and that the  $O_2(b^1\Sigma_g^+)$  in  
 156 photochemical equilibrium, we can write its concentration as a ratio of production to the loss  
 157 term:

$$[O_2(b^1\Sigma_g^+)] = \frac{\varepsilon k_1 [O]^2 M}{A_2 + k_2^{O_2} [O_2] + k_2^{N_2} [N_2] + k_2^O [O]}, \quad (1)$$

158 where  $k_1$  – reaction rate for three-body recombination of atomic oxygen,  $\varepsilon$  is the  
 159 corresponding quantum yield of  $O_2(b^1\Sigma_g^+)$  formation,  $A_2$  represents the spontaneous emission  
 160 coefficient, and  $k_2^{O_2}, k_2^{N_2}, k_2^O$  are the quenching coefficients for reactions with  $O_2, N_2$  and  $O$ ,  
 161 respectively.

162 In case of known temperature, volume emission and concentrations of  $O, O_2, N_2$ , and  $M$ , the  
 163 quantum yield of  $O_2(b^1\Sigma_g^+)$  formation can be calculated as follows:

$$\varepsilon = V_{at} \frac{A_2 + k_2^{O_2} [O_2] + k_2^{N_2} [N_2] + k_2^O [O]}{A_1 k_1 [O]^2 M}, \quad (2)$$

164 where  $A_1$  is spontaneous emission for reaction R5 (hereafter, nomenclature RX means the  
 165 reaction X from Table 1).

166 In the case of the two-step mechanism, the unknown excited state  $O_2^*$  is populated at the first  
 167 step from the reaction R7. Then, it can be deactivated by quenching (R9), spontaneous  
 168 emission (R10) or producing  $O_2(b^1\Sigma_g^+)$  by the reaction R8. Note, R8 is one pathway of the  
 169 overall quenching reaction R9.

170 In the second step,  $O_2^*$  is transformed into  $O_2(b^1\Sigma_g^+)$ , which, can be deactivated by quenching  
 171 (R2-R4) and by spontaneous emission (R6). Assuming photochemical equilibrium for  $O_2^*$  and,  
 172 as before, for  $O_2(b^1\Sigma_g^+)$  the volume emission in the case of  $O_2(b^1\Sigma_g^+ - X^3\Sigma_g^-)(0,0)$  is:

$$V_{at} = \frac{A_1 \alpha k_1 [O]^2 M \gamma k_3^{O_2} [O_2]}{(A_2 + k_2^{O_2} [O_2] + k_2^{N_2} [N_2] + k_2^O [O]) (A_3 + k_3^{O_2} [O_2] + k_3^{N_2} [N_2] + k_3^O [O])}, \quad (3)$$

173 where quantum yield of  $O_2^*$  formation  $\alpha$ , quantum yield of  $O_2(b^1\Sigma_g^+)$  formation  $\gamma$ ,  
 174 spontaneous emission coefficient  $A_3$ , and  $k_3^{O_2}, k_3^{N_2}, k_3^O$  unknown quenching rates of  $O_2^*$ . Note,  
 175 assumption about photochemical equilibrium for  $O_2^*$  and  $O_2(b^1\Sigma_g^+)$  is valid, because  
 176  $O_2(b^1\Sigma_g^+)$  radiative lifetime is less than 12 s and all potential candidates for of  $O_2^*$  have  
 177 lifetime less than several seconds (e.g. López-González et al., 1992a, 1992b, 1992c;  
 178 Yankovsky et al., 2016, and references therein).

179 Collecting all known values on the right-hand side (RHS) and all unknown summands on the  
 180 left-hand side (LHS), omitting emissive summand  $A_3$  as non-effective loss (McDade et al.,  
 181 1986) equation (3) can be rearranged as follows:

$$C^{O_2}[O_2] + C^O[O] = \frac{A_1 k_1 [O]^2 M [O_2]}{V_{at} (A_2 + k_2^{O_2} [O_2] + k_2^{N_2} [N_2] + k_2^O [O])}, \quad (4)$$

182 where  $C^{O_2} = (1 + k_3^{N_2} [N_2] / k_3^{O_2} [O_2]) / \alpha \gamma$  and  $C^O = k_3^O / \alpha \gamma k_3^{O_2}$  are the fitting coefficients  
 183 that can be calculated by the least square fit (LSF) procedure. Such derivation assumes that  
 184 the coefficients are temperature independent (or temperature dependence is weak). This  
 185 means that the reaction rates  $k_3$  are assumed to be temperature independent (dependence is  
 186 weak), or have the same temperature dependency for all quenching partners ( $N_2$ ,  $O_2$ ,  $O$ ).  
 187 Currently, this statement on the basis of available information about potential precursors is  
 188 submitted true, but for which the solid evidence is absent. We calculated them based on our  
 189 measurements and will discuss the results in the following section.

190 In more general case population of  $O_2(b^1\Sigma_g^+)$  occurs via both channels: one-step and two-  
 191 step. We discuss such ability in section 4.3 and derive an expression for corresponding fit-  
 192 function in Appendix.

193

#### 194 **4. Results and Discussion**

195

196 Figure 1 shows input data for our calculations: temperature from CONE instrument (Fig. 1a),  
197 number density of air (Fig. 1b), atomic oxygen concentration measured by FIPEX (Fig. 1c)  
198 and volume emission at 762 nm from photometric instrument (Fig. 1d). A temperature  
199 minimum of  $\sim 158$  K was observed at 104.2 km. A local temperature peak was measured at  
200 98.9 km with values of 204.5 K. The secondary temperature minimum was visible at 95.4 km  
201 and amounted to  $\sim 173$  K. Atomic oxygen concentration (Fig. 1c) had a peak of  $\sim 4.7 \cdot 10^{11}$  [cm<sup>-3</sup>]  
202 <sup>3</sup>] at 97.2 km and approximately coincided with the secondary temperature peak. The peak of  
203 volume emission was detected between 95 and 97 km with values of more than 1700  
204 [phot. $\cdot$ cm<sup>-3</sup> $\cdot$ s<sup>-1</sup>]; this is slightly beneath the atomic oxygen corresponding maximum and  
205 slightly above the secondary temperature minimum. Note, this point to the competition of the  
206 temperature and the atomic oxygen concentration in the processes of atomic oxygen excited  
207 state  $O_2(b^1\Sigma_g^+)$  formation. Independently of the mechanism of atmospheric band emission  
208 (Eq. 1 or Eq. 3), the numerator is directly proportional to the square of atomic oxygen  
209 concentration and inversely proportional to the third power of the temperature (via reaction  
210 rate  $k_I$  and  $M$ , considering the ideal gas law). Our rocket experiment shows an essential  
211 difference of emissions between ascending and descending flights (see Strelnikov et al.,  
212 2018). It also demonstrates a significant variability in other measured parameters, including  
213 neutral temperature and density as well as atomic oxygen density (Strelnikov et al., 2017,  
214 2018). This suggests that, in the case of the ETON 2 experiments, the temporal extrapolation  
215 of atomic oxygen for the time of the emission measurement flight (which was approximately  
216 20 min earlier) may lead to serious biases in estimations because, as one can see from Eq. 1  
217 and Eq. 3, volume emission depends on the atomic oxygen concentration quadratically. Since  
218 the best quality data were obtained during the descent of the WADIS-2 rocket flight, we chose  
219 this data set for our analysis (Strelnikov et al., 2018). The region above 104 km is subject to  
220 auroral contamination. In the region below 92 km, negative values may occur in the volume  
221 emission profile as the result of self-absorption in the denser atmosphere below the emission

222 layer. Hence, we considered the region near the peak of emission between 92 km and 104 km  
223 as most appropriate for our study. The comparisons of our measurements with other  
224 observations, as well as with the results of modelling are presented in several papers (e.g.  
225 Eberhart et al., 2018; Strelnikov et al., 2018).

226

#### 227 **4.1 One-step mechanism**

228

229 Figure 2 shows the quantum yield of  $O_2(b^1\Sigma_g^+)$  formation  $\varepsilon$  calculated according to Eq. (2),  
230 which is necessary to form  $O_2(b^1\Sigma_g^+)$  under the assumption that the direct three-body  
231 recombination of atomic oxygen is the main mechanism. The uncertainties for this figure (as  
232 well as for other figures) were calculated according with sensitivity analysis (von Clarmann,  
233 2014; Yankovsky and Manuilova, 2018, (Appendix 1); Vorobeva et al., 2018). Calculated  
234 values of  $\varepsilon$  are placed in the range [0.07; 0.13], which is in good agreement with the values  
235 derived by McDade et al. (1986). The averaged value amounts to  $0.11\pm 0.018$ . The range of  
236 values taking into account both the variance and the error range amounts to [0.02; 0.22]. By  
237 the physical nature of this value, the quantum yield of  $O_2(b^1\Sigma_g^+)$  formation should not depend  
238 on altitude. Fig. 2 shows some altitude dependence of central values of  $\varepsilon$ , but considering the  
239 large error range, there is no clear altitude dependence. The variability of the data points is  
240 much smaller than the errors of the individual points. Hence, in light of the analysis of our  
241 rocket experiment, we may not decline direct excitation mechanism.

242 Although the population via one-step mechanism alone is, generally speaking, possible, it is  
243 improbable because laboratory experiments show that the direct excitation alone may not  
244 explain observed emissions (Young and Sharpless, 1963; Clyne et al., 1965; Young and  
245 Black, 1966; Bates, 1988). This conclusion is in agreement with the conclusion from McDade  
246 et al. (1986), which stated that the one-step excitation mechanism is not sufficient to explain

247 the  $O_2(b^1\Sigma_g^+)$  population. Hence, in the following, we check the second energy transfer  
248 mechanism.

249

## 250 **4.2 Two-step mechanism**

251

252 Figure 3 depicts the altitude profile of the right hand side (RHS) of equation (4) and profile  
253 calculated by the least-square fit (LSF). The fitting coefficients,  $C^{O_2}$  and  $C^O$ , resulting from  
254 this fit, amount to  $9.8_{+6.5}^{-5.3}$  and  $2.1_{-0.6}^{+0.3}$ , respectively. The uncertainties were calculated, as  
255 commonly for LSF (Bevington and Robinson, 2003), based on error propagation from the  
256 error and variance of RHS as provided in Figure 3. Our  $C^{O_2}$  coefficient is partially, within the  
257 error range, in agreement with  $C^{O_2}$  coefficients given in McDade et al. (1986), which amount  
258 to  $4.8\pm 0.3$  and  $6.6\pm 0.4$  for temperature from CIRA-72 and MSIS-83, respectively. The  $C^O$   
259 coefficient is approximately one order lower. There are several possible reasons for the large  
260 discrepancy in  $C^O$ , for example the temperature dependence of the O-quenching or that, in the  
261 case of ETON 2 experiments mean temperature profiles from the models CIRA-72 and MSIS-  
262 83 were utilized, which does not reproduce any short-time dynamical fluctuations, solar cycle  
263 conditions, etc. In frame of our analysis, we may not identify the reason for the large  
264 discrepancy in  $C^O$  more precisely. Fitting coefficients defined in such a way (Eq. 4) do not  
265 have a direct physical meaning. However, they have a physical meaning in several limit cases.  
266 If the quenching coefficients of a precursor with molecular nitrogen are much smaller than  
267 those with molecular oxygen ( $k_3^{N_2} \ll k_3^{O_2}$ ), then  $\alpha\gamma = 1/C^{O_2}$ . The assumption, that the  
268 quenching of the precursor with  $N_2$  is much slower than quenching with  $O_2$ , is just working  
269 hypothesis, which is commonly used for analysis of possible precursor (e.g. McDade et al.,  
270 1986; López-González et al, 1992a, 1992b; and references therein). It is true for such potential  
271 precursor as  $O_2(A^3\Sigma_u^+)$  (Kenner and Ogryzlo, 1983b), but generally, there is no evidence,  
272 neither for nor against that. If it is not true, any definite conclusion on precursor by known

273  $C^{O_2}$  is not possible. In our case  $\alpha\gamma = 0.102_{-0.041}^{+0.120}$ . In other words, in the case of two-step  
 274 formation of  $O_2(b^1\Sigma_g^+)$  with energy transfer agent  $O_2$ , the total efficiency  $\eta = \alpha\gamma$  amounts to  
 275 10.2%, which is the lowest amongst known values. Based on rocket experiment data analysis  
 276 (ETON), Witt et al. (1984) obtained  $\alpha\gamma = 0.12 - 0.2$ . According to McDade et al. (1986), for  
 277 the case with  $k_2^O = 8 \cdot 10^{-14}$ , the total efficiencies are 0.15 and 0.21 for temperature profiles  
 278 adopted from MSIS-83 and CIRA-72, respectively. The analyses of López-González et al.  
 279 (1992a, c), adopted  $O_2$ ,  $N_2$ , and temperature profiles from the model (Rodrigo et al., 1991),  
 280 showed a total efficiency of 0.16. In contrast to our work, all investigations mentioned above  
 281 utilised the temperature and atmospheric density from models which describe a mean state of  
 282 the atmosphere. This is a possible reason for discrepancy in the results. Total efficiency  $\eta$  may  
 283 serve as an auxiliary quantity to identify the precursor. According to the physical meaning of  
 284 efficiency, it may not be larger than 1. Hence,  $\alpha$ ,  $\gamma$ , as well as the total efficiency are smaller  
 285 than 1. Consequently,  $\gamma = \eta/\alpha < 1$ , and we can examine potential candidates for  $O_2^*$  with this  
 286 criterion. From an energetic point of view, only four bound states of molecular oxygen can be  
 287 considered as an intermediate state for the  $O_2(b^1\Sigma_g^+)$  population:  
 288  $O_2(A^3\Sigma_u^+)$ ,  $O_2(A'^3\Delta_u)$ ,  $O_2(c^1\Sigma_u^-)$ , and  $O_2(^5\Pi_g)$  (Greer et al., 1981; Wraight, 1982; Witt et al.,  
 289 1984; McDade et al., 1986; López-González et al., 1992c). For better readability, we will  
 290 partially repeat a table from López-González et al. (1992b, c) with known  $\alpha$  in our work  
 291 (Table 2). From Table 2, it can be seen that only  $O_2(A'^3\Delta_u)$  and  $O_2(^5\Pi_g)$  fit to the criterion of  
 292  $\gamma = 0.102/\alpha < 1$ . At lower limit of uncertainty ( $\gamma = 0.061/\alpha < 1$ )  $O_2(A'^3\Delta_u)$  and  $O_2(^5\Pi_g)$   
 293 satisfy to the criterion, and considering upper limit ( $\gamma = 0.222/\alpha < 1$ ), only  $O_2(^5\Pi_g)$  may  
 294 serve as precursor.

295 The second expression that helps to clarify the choice of the precursor is the ratio of  
 296 quenching rates. In the limit of low quenching with molecular nitrogen ( $k_3^{N_2} \ll k_3^{O_2}$ ), the ratio  
 297 of fitting coefficients equals the ratio of the quenching rates of atomic and molecular oxygens

298  $(C^O/C^{O_2} = k_3^O/k_3^{O_2})$ . An analysis from the ETON 2 rocket experiment yields values of  
 299 quenching coefficients ratios of potential precursor of 3.1 and 2.9 for temperatures from  
 300 CIRA-72 and MSIS-83, respectively. This is close to the value from Ogryzlo et al. (1984),  
 301 who found  $k_3^O/k_3^{O_2} = 2.6$  by laboratory measurements; however, as was noted in their work,  
 302 substitution of these values into the equation for emission yields 16 % of the observed  
 303 emission (Ogryzlo et al., 1984). These findings point to the possibility of a too high measured  
 304 ratio  $k_3^O/k_3^{O_2}$  as the result of too strong quenching of precursor by atomic oxygen. Our value  
 305 of quenching ratios  $k_3^O/k_3^{O_2}$  amounts to  $0.21_{-0.12}^{+0.32}$ . There is not enough information on  
 306 measured values for bound states of molecular oxygen. Laboratory measurements for  
 307  $O_2(A^3\Sigma_u^+)(v = 0 - 4)$ ,  $O_2(A^3\Sigma_u^+)(v = 2)$ , and  $O_2(c^1\Sigma_u^-)$  infer the values of  $k_3^O/k_3^{O_2}$  ratio to  
 308 be  $30\pm 30$ ,  $100\pm 15$ , and  $200\pm 20$ , respectively (Kenner and Ogryzlo, 1980; Kenner and  
 309 Ogryzlo, 1983a, 1983b; Kenner and Ogryzlo, 1984). On the other hand, Slanger et al. (1984)  
 310 found a lower limit of  $O_2(A^3\Sigma_u^+)(v = 8)$  quenching by  $O_2$  must be  $\geq 8 \cdot 10^{-11}$ . If the results  
 311 from Slanger et al. (1984) were applied to the results from Kenner and Ogryzlo (1980, 1984)  
 312 for  $k_3^{O_2}$ , then the ratio of  $k_3^O/k_3^{O_2}$  would be two orders lower. This short discussion illustrates a  
 313 strong scattering of this ratio. For our two potential candidates ( $O_2(A'^3\Delta_u)$  and  $O_2(^5\Pi_g)$ ),  
 314 there is information about  $k_3^O/k_3^{O_2}$  ratio for only  $O_2(A'^3\Delta_u)$ . Through the comprehensive  
 315 analysis of known rocket experiments, López-González et al. (1992a, b, c) inferred that the  
 316 upper limit of the ratio amounts to 1. Hence, our value of  $k_3^O/k_3^{O_2} = 0.21_{-0.12}^{+0.32}$  agrees with  
 317 this result. Consistent information from laboratory experiments on the ratio for  $O_2(^5\Pi_g)$  is  
 318 absent. Thus, we can propose as potential candidates for precursor both  $O_2(A'^3\Delta_u)$  and  
 319  $O_2(^5\Pi_g)$ ; however, we are not able to identify which of these two is more preferable.

320 In order to illustrate the application of the newly derived fitting coefficients we compare in  
 321 Figure 4 the atomic oxygen concentration from FIPEX (black line), from NRL MSISE-00  
 322 reference atmosphere model (Picone et al., 2002) (red line); calculated with McDade et al.

323 (1986) coefficients (blue line), and with our fitting coefficients for the two-step mechanism  
 324 (green line). In the region 94-98 km, i.e. at atomic oxygen peak and volume emission peak  
 325 (see Fig. 1d) fitting coefficients from this paper better than McDade coefficients (MSIS-83  
 326 case) reproduce observed values. Our fitting coefficients and fitting coefficients of McDade  
 327 give similar approximation above atomic oxygen peak (~98-104 km). The shape of the  
 328 calculated profiles appears slightly different, with the peak maximum at a higher altitude than  
 329 the observed. In this, our result resembles the McDade results, probably because in both  
 330 cases, the ratio of two reaction rates is derived, but not the rates themselves. In the lower part  
 331 our results and those of McDade differ, because our  $C^{O_2}$  value is larger and term with  
 332 molecular oxygen dominates. Nevertheless, the atomic oxygen retrieved with our fitting  
 333 coefficients satisfactorily reproduces measurements, especially at the peak.

334

### 335 **4.3 Combined mechanism**

336

337 In the most general case, the  $O_2(b^1\Sigma_g^+)$  population passes through two channels: directly and  
 338 via precursor. In fact, theoretical calculations from Wraight (1982) and laboratory  
 339 measurements from Bates (1988) predicted a direct population with efficiencies of 0.015 and  
 340 0.03, respectively, which is not sufficient to explain the observed emissions (Bates, 1988,  
 341 Greer et al., 1981; Krasnopolsky, 1986). A similar value,  $\epsilon=0.02$ , was shown in the analysis  
 342 by López-González et al. (1992b, c). We investigated a combined mechanism based on the  
 343 LSF calculation and fit function (derivation in Appendix):

$$\frac{[O_2] + D_1[O]}{D_2 + \tilde{\epsilon}(1 + D_1[O]/[O_2])} = \frac{A_1 k_1 [O]^2 M [O_2]}{V_{at}(A_2 + \tilde{k}_2^{O_2} [O_2] + \tilde{k}_2^{N_2} [N_2] + \tilde{k}_2^O [O])}, \quad (5)$$

344 where, hereafter, tildes denote that these are values for combined mechanism and do not equal  
 345 to the values for one-step or two-step mechanisms (Sec. 4.1 and 4.2);  $D_1 = \tilde{k}_3^O / \tilde{k}_3^{O_2}$  and  
 346  $D_2 = \tilde{\alpha}\tilde{\gamma}$  are the fitting coefficients, which refer to the ratio of quenching rates and  $\tilde{\eta} \equiv \tilde{\alpha}\tilde{\gamma}$

347 total efficiency for two-step channel, respectively. The fitting coefficients were calculated for  
348 two limit cases  $\tilde{\epsilon}=0.015$  (Wraight, 1982),  $\tilde{\epsilon}=0.03$  (Bates, 1988) and for the averaged case  
349  $\tilde{\epsilon}=0.022$ .

350 The results for the best-fit in each case are listed in Table 3. Analogously to the two-step  
351 mechanism (Sec. 4.2), for the case of combined mechanism  $\tilde{\gamma} = \tilde{\eta}/\tilde{\alpha} < 1$ , hence, the  
352 precursor should satisfy  $\tilde{\alpha} > 0.08_{-0.04}^{+0.12}$  (see Tab. 3). For central values of  $\tilde{\alpha}$ , only  $O_2(A'^3\Delta_u)$   
353 and  $O_2(^5\Pi_g)$  satisfy this criterion (see Tab. 2). At lower limit of uncertainty ( $\tilde{\alpha} >$   
354  $0.04$ )  $O_2(A'^3\Delta_u)$ ,  $O_2(A^3\Sigma_u^+)$ , and  $O_2(^5\Pi_g)$  satisfy to the criterion, and considering upper limit  
355 ( $\tilde{\alpha} > 0.2$ ), only  $O_2(^5\Pi_g)$  may serve as precursor. The upper limit of the ratio  $k_3^0/k_3^{02} < 1$  for  
356  $O_2(A'^3\Delta_u)$ , derived by López-González et al. (1992a, b, c), is in agreement with our  
357 calculations ( $0.231_{-0.142}^{+0.358}$ ). As it is noted above, the ratio for  $O_2(^5\Pi_g)$  is unknown.  
358 Consequently, taking into an account both conditions, only  $O_2(A'^3\Delta_u)$  and  $O_2(^5\Pi_g)$  may  
359 serve as precursor.

360 Figure 5 illustrates a sanity check for volume emissions derived (black lines) with fitting  
361 coefficients of McDade et al. (1986) for MSIS-83 (Fig. 5c) case and CIRA-72 case (Fig. 5d),  
362 and with our newly derived fitting coefficients for two-step (Fig. 5a) and combined ( $\tilde{\epsilon} =$   
363  $0.022$ ) mechanisms (Fig. 5b) in comparison with measured one (red lines). All of derived  
364 volume emission profiles (black lines) were calculated based on the temperature,  
365 concentration of surrounding air, and concentration of atomic oxygen from our rocket launch.  
366 The calculations with combined mechanism (Eq. 5) and two-step energy transfer mechanism  
367 (Eq. 4) give almost identical results. The results obtained with new fitting coefficients are in  
368 satisfactory agreement with the measured volume emissions at the peak and above, whereas  
369 the McDade coefficients related to the temperature from CIRA-72 give better approximations  
370 below the volume emission peak (92 km). The coefficients of McDade related to the  
371 temperature from MSIS-83 are in better agreement with our results and are almost identical

372 above the volume emission peak. More independent common volume in-situ measurements  
373 are necessary to validate these results.

374

## 375 **5. Summary and conclusions**

376

377 Based on the rocket-born common volume simultaneous observations of atomic oxygen,  
378 atmospheric band emission (762 nm), and density and temperature of the background  
379 atmosphere, the mechanisms of  $O_2(b^1\Sigma_g^+)$  formation were analysed. Our calculations show  
380 that one-step direct excitation is less probable by the reasons discussed above (Sec. 4.1).

381 For the case of the two-step mechanism, we found new coefficients for fit function in  
382 accordance with McDade et al. (1986), based on self-consistent temperature, atomic oxygen  
383 and volume emission observation. These coefficients amounted to  $C^{O_2}=9.8_{+6.5}^{-5.3}$  and  
384  $C^O=2.1_{-0.6}^{+0.3}$ .  $C^{O_2}$  coefficient is partially, within the error range, in agreement with  $C^{O_2}$   
385 coefficients given in McDade et al. (1986), and  $C^O$  coefficient is approximately one order  
386 lower. The general implication of these results is parameterisation of volume emission in  
387 terms of known atomic oxygen. This can be utilised either for atmospheric band volume  
388 emission modelling or for estimation of atomic oxygen by known volume emission. We  
389 identified two candidates for the intermediate state of  $O_2^*$ . Our results show that  $O_2(A'^3\Delta_u)$  or  
390  $O_2(^5\Pi_g)$  may serve as a precursor.

391 Taking into account both channels of  $O_2(b^1\Sigma_g^+)$  formation, we proposed a combined  
392 mechanism. In this case, atomic oxygen via volume emission or volume emission based on  
393 known atomic oxygen can be calculated by equation (5). Recommended fitting coefficients  
394 amounted to  $D_1=0.231_{-0.142}^{+0.358}$  and  $D_2=0.08_{-0.04}^{+0.12}$ , with the efficiency of the direct channel as  
395  $\tilde{\epsilon} = 0.022$ . These coefficients have a meaning of total efficiency ( $\tilde{\alpha}\tilde{\gamma}$ ) and a ratio of  
396 quenching coefficients ( $\tilde{k}_3^O/\tilde{k}_3^{O_2}$ ) for the two-step channel. The analysis of their values

397 indicates that  $O_2(A'^3\Delta_u)$  and  $O_2(^5\Pi_g)$  may serve as possible precursors for the two-step  
 398 channel at combined mechanism. In the context of our rocket experiment, we do not have the  
 399 possibility to figure out which mechanism is true. Nevertheless, we consider the combined  
 400 mechanism as more relevant to nature, because it has a higher generality. This conclusion  
 401 does not contradict to the current point of view that the two-step mechanism is dominant  
 402 because  $\tilde{\varepsilon}$  is assumed to be 1.5-3 %. Moreover, it is possible that in the reality the mechanism  
 403 is much more complex and it has multi-channel or more than two-step nature. Undoubtedly,  
 404 more common volume simultaneous observations of the Atmospheric Band and the atomic  
 405 oxygen concentrations would be desirable to confirm and improve these results.

406

#### 407 **Appendix.**

408

409 We consider photochemical equilibrium for the night-time  $O_2(b^1\Sigma_g^+)$  concentration. If  
 410  $O_2(b^1\Sigma_g^+)$  is produced via both channels, the equilibrium concentration is given by the  
 411 following expression:

$$[O_2(b^1\Sigma_g^+)] = \frac{\tilde{\varepsilon}k_1[O]^2M + \tilde{\gamma}\tilde{k}_3^{O_2}[O_2][O_2^*]}{A_2 + k_2^{O_2}[O_2] + k_2^{N_2}[N_2] + k_2^O[O]}, \quad (A1)$$

412 where the tilde denotes the combined mechanism,  $A_1, k_1, k_2^{O_2}, k_2^{N_2}, k_2^O, \tilde{k}_3^{O_2}$  are the ratios for  
 413 corresponding processes (see Tab. 1) and  $O_2^*$  is the unknown precursor.

414 Considering this precursor in photochemical equilibrium, we can obtain the following  
 415 expression for its concentration:

$$[O_2^*] = \frac{\tilde{\alpha}k_1[O]^2M}{\tilde{A}_3 + \tilde{k}_3^{O_2}[O_2] + \tilde{k}_3^{N_2}[N_2] + \tilde{k}_3^O[O]}, \quad (A2)$$

416 where efficiency  $\tilde{\alpha}$ ,  $\tilde{A}_3$  is the unknown spontaneous emission coefficient of  $O_2^*$  and  
 417  $\tilde{k}_3^{O_2}, \tilde{k}_3^{N_2}, \tilde{k}_3^O$  are the unknown quenching rates for  $O_2^*$ .

418 Substituting A2 into A1 and into expression for volume emission we obtain:

419  $V_{at} = A_1[O_2(b^1\Sigma_g^+)] =$

$$= \frac{A_1 k_1 [O]^2 [O_2] M}{A_2 + k_2^{O_2} [O_2] + k_2^{N_2} [N_2] + k_2^O [O]} \left( \frac{\tilde{\varepsilon}}{[O_2]} + \frac{\tilde{\alpha}\tilde{\gamma}\tilde{k}_3^{O_2}}{\tilde{A}_3 + \tilde{k}_3^{O_2} [O_2] + \tilde{k}_3^{N_2} [N_2] + \tilde{k}_3^O [O]} \right). \quad (A3)$$

420 We assume that, in analogy with two-step mechanism, a spontaneous emission  $\tilde{A}_3$  of  $O_2^*$  is  
 421 much smaller than the quenching, and we utilised traditional assumption about low quenching  
 422 with molecular nitrogen ( $\tilde{k}_3^{N_2} \ll \tilde{k}_3^{O_2}$ ), which is commonly used to analyse a potential  
 423 precursor. In this case, A3 can be rearranged as follows:

$$\frac{[O_2] + \frac{\tilde{k}_3^O}{\tilde{k}_3^{O_2}} [O]}{\tilde{\alpha}\tilde{\gamma} + \tilde{\varepsilon} \left( 1 + \frac{\tilde{k}_3^O}{\tilde{k}_3^{O_2}} [O]/[O_2] \right)} = \frac{A_1 k_1 [O]^2 M [O_2]}{V_{at} (A_2 + k_2^{O_2} [O_2] + k_2^{N_2} [N_2] + k_2^O [O])}. \quad (A4)$$

424 We defined unknown fitting coefficients  $D_1 \equiv \tilde{k}_3^O/\tilde{k}_3^{O_2}$  and  $D_2 \equiv \tilde{\alpha}\tilde{\gamma}$ . Expression A4 was  
 425 utilised to calculate them with LSF.

426

## 427 **Acknowledgements.**

428

429 The authors are thankful to Prof. Dr. V. A. Yankovsky, Prof. Dr. W. Ward, and PD Dr. G. R.  
 430 Sonnemann for helpful suggestions and useful discussions. This work was supported by the  
 431 German Space Agency (DLR) under grant 50 OE 1001 (project WADIS). The authors thank  
 432 DLR-MORABA for their excellent contribution to the project by developing the complicated  
 433 WADIS payload and campaign support together with the Andøya Space Center, as well as H.-  
 434 J. Heckl and T. Köpnick for building the rocket instrumentation.

435 The rocket-borne measurements and calculated data shown in this paper are available via  
 436 IAP's ftp server at <ftp://ftp.iap-kborn.de/data-in-publications/GrygalashvylyACP2018>.

437

## 438 **References**

439

440 Bates, D. R.: Excitation and quenching of the oxygen bands in the nightglow, *Planet. Space*  
441 *Sci.*, **36(9)**, 875-881, 1988.

442

443 Becker, E., and Vadas, S. L.: Secondary gravity waves in the winter mesosphere: Results  
444 from a high-resolution global circulation model, *J. Geophys. Res.*, **123**, 2605-2627,  
445 doi:10.1002/2017JD027460, 2018.

446

447 Bevington, P. R., and Robinson, D. K.: Data reduction and error analysis for the physical  
448 sciences, 3rd edition, published by McGraw-Hill Companies Inc., ISBN 0-07-247227-8,  
449 2003.

450

451 Campbell, I. M. and Gray, C. N.: Rate constants for  $O(^3P)$  recombination and association with  
452  $N(4S)$ , *Chem. Phys. Lett.*, **8**, 259, 1973.

453

454 von Clarmann, T.: Smoothing error pitfalls, *Atmos. Meas. Tech.*, **7**, 3023-3034,  
455 <https://doi.org/10.5194/amt-7-3023-2014>, 2014.

456

457 Clyne, M. A. A., Thrush, B. A., and Wayne, R. P.: The formation and reactions of metastable  
458 oxygen ( $b^1\Sigma_g^+$ ) molecules, *J. Photochem. Photobiol.*, **4**, 957, 1965.

459

460 Deans, A. J., Shepherd, G. G., and Evans, W. F. J.: A rocket measurement of the  $O_2(b^1\Sigma_g^+ -$   
461  $X^3\Sigma_g^-)$  atmospheric band nightglow altitude distribution, *Geophys. Res. Lett.*, **3(8)**, 441-444,  
462 1976.

463

464 Eberhart, M., Löhle, S., Steinbeck, A., Binder, T., and Fasoulas, S.: Measurement of atomic  
465 oxygen in the middle atmosphere using solid electrolyte sensors and catalytic probes,  
466 *Atmospheric Measurement Techniques*, **8**, 3701–3714, doi:10.5194/amt-8-3701-2015, 2015.

467

468 Eberhart, M., Löhle, S., Strelnikov, B., Fasoulas, S. and Lübken, F.-J. Hedin, J., Khaplanov,  
469 M., Gumbel, J.: Atomic oxygen number densities in the MLT region measured by solid  
470 electrolyte sensors on WADIS-2, *Atmospheric Measurement Techniques*, submitted, 2018.

471

472 Giebeler, J., Lübken, F.-J., and Nägele, M.: CONE – a new sensor for in-situ observations of  
473 neutral and plasma density fluctuations, ESA SP, Montreux, Switzerland, ESA-SP-355, 311–  
474 318, 1993.

475

476 Greer, R. G. H., Llewellyn, E. J., Solheim, B. H., and Witt, G.: The excitation of  $O_2(b^1\Sigma_g^+)$  in  
477 the nightglow, *Planet. Space Sci.*, **29**, 383, 1981.

478

479 Hedin, A. E.: A revised thermospheric model based on mass spectrometer and incoherent  
480 scatter data: MSIS-83, *J. Geophys. Res.*, **88**, 10.170, 1983.

481

482 Hedin, J., Gumbel, J., Stegman, J., and Witt, G.: Use of  $O_2$  airglow for calibrating direct  
483 atomic oxygen measurements from sounding rockets, *Atmos. Meas. Tech.*, **2**, 801–812, 2009.

484

485 Hickey, M. P., Schubert, G., and Walterscheid, R. L.: Gravity wave-driven fluctuations in the  
486  $O_2$  atmospheric (0–1) nightglow from an extended, dissipative emission region, *J. Geophys.*  
487 *Res.*, **98**, 717–730, 1993.

488

489 Kenner, R. D. and Ogryzlo, E. A.: Deactivation of  $O_2(A^3\Sigma_u^+)$  by  $O_2$ , O and Ar, *Int. J. Chem.*  
490 *Kinetics*, **12**, 501, 1980.

491

492 Kenner, R. D. and Ogryzlo, E. A.: Quenching of  $O_2(c^1\Sigma_u^-, v = 0)$  by  $O(^3P)$ ,  $O_2(a^1\Delta_g)$  and  
493 other gases, *Can. J. Chem.*, **61**, 921, 1983a.

494

495 Kenner, R. D. and Ogryzlo, E. A.: Rate constant for the deactivation of  $O_2(A^3\Sigma_u^+)$  by  $N_2$ ,  
496 *Chem. Phys. Lett.*, **103**, 209, 1983b.

497

498 Kenner, R. D. and Ogryzlo, E. A.: Quenching of  $O_2(A_{v=2} - X_{v=5})$  Herzberg I band by  $O_2(a)$   
499 and O, *Can. J. Phys.*, **62**, 1599, 1984.

500

501 Krasnopolsky, V. A.: Oxygen emissions in the night airglow of the Earth, Venus and Mars,  
502 *Planet. Space Sci.*, **34**, 511, 1986.

503

504 Leko, J. J., M. P. Hickey, and Richards, P. G.: Comparison of simulated gravity wave-driven  
505 mesospheric airglow fluctuations observed from the ground and space, *J. Atmos. Solar-Terr.*  
506 *Phys.*, **64**, 397–403, 2002.

507

508 Liu, A. Z. and Swenson, G. R.: A modeling study of  $O_2$  and OH airglow perturbations  
509 induced by atmospheric gravity waves, *J. Geophys. Res.*, **108(D4)**, 4151,  
510 doi:10.1029/2002JD002474, 2003.

511

512 López-González, M. J., López-Moreno, J. J., and Rodrigo, R.: Altitude profiles of the  
513 atmospheric system of  $O_2$  and of the green line emission, *Planet. Space Sci.*, **40(6)**, 783-795,  
514 1992a.

515

516 López-González, M. J., López-Moreno, J. J., and Rodrigo, R.: Altitude and vibrational  
517 distribution of the O<sub>2</sub> ultraviolet nightglow emissions, *Planet. Space Sci.*, **40(7)**, 913-928,  
518 1992b.

519

520 López-González, M. J., López-Moreno, J. J., and Rodrigo, R.: Atomic oxygen concentrations  
521 from airglow measurements of atomic and molecular oxygen emissions in the nightglow,  
522 *Planet. Space Sci.*, **40(7)**, 929-940, 1992c.

523

524 Lopez-Gonzalez, M. J., Rodríguez, E., Shepherd, G. G., Sargoytchev, S., Shepherd, M. G.,  
525 Aushev, V. M., Brown, S., García-Comas, M., and Wiens, R. H.: Tidal variations of O<sub>2</sub>  
526 Atmospheric and OH(6-2) airglow and temperature at mid-latitudes from SATI observations,  
527 *Ann. Geophys.*, **23**, 3579–3590, 2005.

528

529 Lopez-Gonzalez, M. J., Rodríguez, E., García-Comas, M., Costa, V., Shepherd, M. G.,  
530 Shepherd, G. G., Aushev, V. M., and Sargoytchev, S.: Climatology of planetary wave type  
531 oscillations with periods of 2-20 days derived from O<sub>2</sub> atmospheric and OH(6-2) airglow  
532 observations at mid-latitude with SATI, *Ann. Geophys.*, **27**, 3645–3662, 2009.

533

534 Lübken, F.-J.: Seasonal variation of turbulent energy dissipation rates at high latitudes as  
535 determined by in situ measurements of neutral density fluctuations, *J. Geophys. Res.*, **102**,  
536 13,441-13,456, 1997.

537

538 McDade, I. C., Murtagh, D. P., Greer, R. G. H., Dickinson, P. H. G., Witt, G., Stegman, J.,  
539 Llewellyn, E. J., Thomas, L., and Jenkins, D. B.: ETON 2: Quenching parameters for the

540 proposed precursors of  $O_2(b^1\Sigma_g^+)$  and  $O(^1S)$  in the terrestrial nightglow, *Planet. Space Sci.*,  
541 **34**, 789–800, 1986.

542

543 Mlynczak, M. G., Morgan, F., Yee, J.-H., Espy, P., Murtagh, D., Marshall, B., Schmidlin, F.:  
544 Simultaneous measurements of the  $O_2(^1\Delta)$  and  $O_2(^1\Sigma)$  airglows and ozone in the daytime  
545 mesosphere, *Geophys. Res. Lett.*, **28**, 999-1002, 2001.

546

547 Murtagh, D. P., Witt, G., Stegman, J., McDade, I. C., Llewellyn, E. J., Harris, F., and Greer,  
548 R. G. H.: An assessment of proposed  $O(^1S)$  and  $O_2(b^1\Sigma_g^+)$  nightglow excitation parameters,  
549 *Planet. Space Sci.*, **38**, 1, 45–53, 1990.

550

551 Newnham, D. A. and Balard, J.: Visible absorption cross sections and integrated absorption  
552 intensities of molecular oxygen ( $O_2$  and  $O_4$ ), *J. Geophys. Res.*, **103(D22)**, 28801-28815, 1998.

553

554 Noxon, J. F.: Effect of Internal Gravity Waves Upon Night Airglow Temperatures, *Geophys.*  
555 *Res. Lett.*, **5**, 25–27, 1978.

556

557 Ogryzlo, E. A., Shen, Y. Q., and Wassel, P. T.: The yield of  $O_2(b^1\Sigma_g^+)$  in oxygen atom  
558 recombination, *J. Photochem.*, **25**, 389, 1984.

559

560 Picone, J. M., Hedin, A. E., Drob, D. P., and Aikin, A. C.: NRLMSISE-00 empirical model of  
561 the atmosphere: Statistical comparisons and scientific issues, *J. Geophys. Res.*, **107**, 1468,  
562 doi:10.1029/2002JA009430, 2002.

563

564 Rapp, M., and Lübken, F.-J.: Polar mesosphere summer echoes (PMSE): Review of  
565 observations and current understanding, *Atmos. Chem. Phys.*, **4**, 2601-2633, 2004

566

567 Rodrigo, R., Lopez-Gonzalez, M. J., and Lopez-Moreno, J. J.: Variability of the neutral  
568 mesospheric and lower thermospheric composition in the diurnal cycle, *Planet. Space Sci.*,  
569 **39**, 803, 1991.

570

571 Sheese, P. E., Llewellyn, E. J., Gattinger, R. L., Bourassa, A. E., Degenstein, D. A., Lloyd, N.  
572 D., and McDade I. C.: Temperatures in the upper mesosphere and lower thermosphere from  
573 OSIRIS observations of O<sub>2</sub> A-band emission spectra, *Can. J. Phys.*, **88**, 919–925,  
574 doi:10.1139/P10-093, 2010.

575

576 Sheese, P. E., Llewellyn, E. J., Gattinger, R. L., Bourassa, A. E., Degenstein, D. A., Lloyd, N.  
577 D., and McDade I. C.: Mesopause temperatures during the polar mesospheric cloud season,  
578 *Geophys. Res. Lett.*, **38**, L11803, doi:10.1029/2011GL047437. 2011.

579

580 Shepherd, M. G., Cho, Y.-M., Shepherd, G. G., Ward, W., and Drummond, J. R.:  
581 Mesospheric temperature and atomic oxygen response during the January 2009 major  
582 stratospheric warming, *J. Geophys. Res.*, **115**, A07318, doi:10.1029/2009JA015172, 2010.

583

584 Slanger, T. G. and Black, G.: Interactions of O<sub>2</sub>(b<sup>1</sup>Σ<sub>g</sub><sup>+</sup>) with O(<sup>3</sup>P) and O<sub>3</sub>. *J. Chem. Phys.*, **70**,  
585 3434-3438, 1979.

586

587 Slanger, T. G., Bischel, W. K., and Dyer, M. J.: Photoexcitation of O<sub>2</sub> at 249.3 nm, *Chem.*  
588 *Phys. Lett.*, **108**, 472, 1984.

589

590 Smith, A. K., Marsh, D. R., Mlynczak, M. G., and Mast J. C.: Temporal variation of atomic  
591 oxygen in the upper mesosphere from SABER, *J. Geophys. Res.*, **115**, D18309,  
592 doi:10.1029/2009JD013434, 2010.

593

594 Smith, I. W. M.: The role of electronically excited states in recombination reactions, *Int. J.*  
595 *Chem. Phys.*, **16**, 423–443, 1984.

596

597 Strelnikov, B., Rapp, M., and Lübken, F.-J.: In-situ density measurements in the  
598 mesosphere/lower thermosphere region with the TOTAL and CONE instruments, in: An  
599 Introduction to Space Instrumentation, edited by: Oyama, K., Terra Publishers,  
600 doi:10.5047/isi.2012.001, 2013. <http://www.terrapub.co.jp/onlineproceedings/ste/aisi/>

601

602 Strelnikov, B., Szewczyk, A., Strelnikova, I., Latteck, R., Baumgarten, G., Lübken, F.-J.,  
603 Rapp, M., Fasoulas, S., Löhle, S., Eberhart, M., Hoppe, U.-P., Dunker, T., Friedrich, M.,  
604 Hedin, J., Khaplanov, M., Gumbel, J., and Barjatya, A.: Spatial and temporal variability in  
605 MLT turbulence inferred from in situ and ground based observations during the WADIS-1  
606 sounding rocket campaign, *Ann. Geophys.*, **35**, 547–565, doi:10.5194/angeo-35-547-2017,  
607 2017.

608

609 Strelnikov, B., Staszak, T., Strelnikova, I., Lübken, F.-J., Grygalashvyly, M., Hedin, J.,  
610 Khaplanov, M., Gumbel, J., Fasoulas, S., Löhle, S., Eberhart, M., Baumgarten, G., Höffner,  
611 J., Wörl, R., Rapp, M., and Friedrich, M.: Simultaneous in situ measurements of small-scale  
612 structures in neutral, plasma, and atomic oxygen densities during WADIS sounding rocket  
613 project, *Atmos. Chem. Phys.*, submitted , 2018.

614

615 Tarasick, D. W. and Shepherd, G. G.: Effects of gravity waves on complex airglow  
616 chemistries. 2. OH emission, *J. Geophys. Res.*, **97**, 3195-3208, 1992.

617  
618 Viereck, R. A. and Deehr, C. S.: On the interaction between gravity waves and the OH Meinel  
619 (6-2) and O<sub>2</sub> Atmospheric (0-1) bands in the polar night airglow, *J. Geophys. Res.*, **94**, 5397–  
620 5404, 1989.

621  
622 Vorobeva, E., Yankovsky, V., and Schayer, V.: Estimation of uncertainties of the results of  
623 [O(<sup>3</sup>P)], [O<sub>3</sub>] and [CO<sub>2</sub>] retrievals in the mesosphere according to the YM2011 model by two  
624 approaches: sensitivity study and Monte Carlo method, EGU General Assembly, Vienna,  
625 Austria, 8–13 April 2018, EGU2018-AS1.31/ST3.7-17950,  
626 [https://presentations.copernicus.org/EGU2018-17950\\_presentation.pdf](https://presentations.copernicus.org/EGU2018-17950_presentation.pdf), 2018.

627  
628 Wildt, J., Bednarek, G., Fink, E. H., Wayne, R. P.: Laser excitation of the A<sup>3</sup>Σ<sub>u</sub><sup>+</sup>, A<sup>3</sup>Δ<sub>u</sub> and  
629 c<sup>1</sup>Σ<sub>u</sub><sup>-</sup> states of molecular oxygen, *Chem. Phys.*, **156(3)**, 497-508, doi: 10.1016/0301-  
630 0104(91)89017-5, 1991.

631  
632 Witt, G., Stegman, J., Murtagh, D. P., McDade, I. C., Greer, R. G. H., Dickinson, P. H. G.,  
633 and Jenkins, D. B.: Collisional energy transfer and the excitation of O<sub>2</sub>(b<sup>1</sup>Σ<sub>g</sub><sup>+</sup>) in the  
634 atmosphere, *J. Photochem.*, **25**, 365, 1984.

635  
636 Wraight, P. C.: Association of atomic oxygen and airglow excitation mechanisms, *Planet.*  
637 *Space Sci.*, **30(3)**, 251-259, 1982.

638  
639 Yankovsky, V. A. and Manuilova, R. O.: Possibility of simultaneous [O<sub>3</sub>] and [CO<sub>2</sub>] altitude  
640 distribution retrievals from the daytime emissions of electronically-vibrationally excited

641 molecular oxygen in the mesosphere, *J. Atmos. Sol.-Terr. Phys.*, **179**, 22-33, doi:  
642 10.1016/j.jastp.2018.06.008, 2018.

643

644 Yankovsky, V. A., Martysenko, K. V., Manuilova, R. O., and Feofilov, A. G.: Oxygen  
645 dayglow emissions as proxies for atomic oxygen and ozone in the mesosphere and lower  
646 thermosphere, *J. Mol. Spectrosc.*, **327**, 209–231, doi:10.1016/j.jms.2016.03.006, 2016.

647

648 Young, R. A. and Sharpless, R. L.: Chemiluminescence and reactions involving atomic  
649 oxygen and nitrogen, *J. Chem. Phys.*, **39**, 1071, 1963.

650

651 Young, R. A. and Black, G.: Excited state formation and destruction in mixtures of atomic  
652 oxygen and nitrogen, *J. Chem. Phys.*, **44**, 3741, 1966.

653

654 Zagidullin, M. V., Khvatov, N. A., Medvedkov, I. A., Tolstov, G. I., Mebel, A. M., Heaven,  
655 M. C., and Azyazov, V. N.: O<sub>2</sub>(b<sup>1</sup>Σ<sub>g</sub><sup>+</sup>) Quenching by O<sub>2</sub>, CO<sub>2</sub>, H<sub>2</sub>O, and N<sub>2</sub> at Temperatures  
656 of 300–800 K, *J. Phys. Chem.*, **121 (39)**, 7343-7348, doi: 10.1021/acs.jpca.7b07885, 2017.

657

658 Zarboo, A., Bender, S., Burrows, J. P., Orphal, J., and Sinnhuber, M.: Retrieval of O<sub>2</sub>(<sup>1</sup>Σ) and  
659 O<sub>2</sub>(<sup>1</sup>Δ) volume emission rates in the mesosphere and lower thermosphere using  
660 SCIAMACHY MLT limb scans, *Atmos. Meas. Tech.*, **11**, 473-487,  
661 <https://doi.org/10.5194/amt-11-473-2018>, 2018.

662

663 Zhang, S. P., Wiens, R. H., and Shepherd, G. G.: Gravity waves from O<sub>2</sub> nightglow during the  
664 AIDA '89 campaign II: numerical modeling of the emission rate/temperature ratio, η, *J.*  
665 *Atmos. Terr. Phys.*, **55**, 377–395, 1993.

666

667 **Table 1.** List of reactions with corresponding reaction rates (for three-body reactions [ $\text{cm}^6$   
668  $\text{molecule}^{-2} \text{s}^{-1}$ ] and for two-body reactions [ $\text{cm}^3 \text{molecule}^{-1} \text{s}^{-1}$ ]), quenching coefficients, and  
669 spontaneous emission coefficients ( $\text{s}^{-1}$ ) used in the paper.

	Reaction	Coefficient	Reference
R1	$O + O + M \xrightarrow{\varepsilon k_1} O_2(b^1\Sigma_g^+) + M$	$k_1 = 4.7 \cdot 10^{-33} (300/T)^2$ $\varepsilon - \text{unknown}$	Campbel and Gray (1973)
R2	$O_2(b^1\Sigma_g^+) + O_2 \xrightarrow{k_2^{O_2}} \text{products}$	$k_2^{O_2}$ $= 7.4 \cdot 10^{-17} T^{0.5} e^{-\frac{1104.7}{T}}$	Zagidullin et al. (2017)
R3	$O_2(b^1\Sigma_g^+) + N_2 \xrightarrow{k_2^{N_2}} \text{products}$	$k_2^{N_2} = 8 \cdot 10^{-20} T^{1.5} e^{\frac{503}{T}}$	Zagidullin et al. (2017)
R4	$O_2(b^1\Sigma_g^+) + O \xrightarrow{k_2^O} \text{products}$	$k_2^O = 8 \cdot 10^{-14}$	Slanger and Black (1979)
R5	$O_2(b^1\Sigma_g^+) \xrightarrow{A_1} O_2 + h\nu(762\text{nm})$	$A_1 = 0.0834$	Newnham and Ballard (1998)
R6	$O_2(b^1\Sigma_g^+) \xrightarrow{A_2} O_2 + h\nu(\text{total})$	$A_2 = 0.088158$	Yankovsky et al. (2016)
R7	$O + O + M \xrightarrow{\alpha k_1} O_2^* + M$	$\alpha - \text{unknown}$	
R8	$O_2^* + O_2 \xrightarrow{\gamma k_3^{O_2}} O_2(b^1\Sigma_g^+) + O_2$	$\gamma - \text{unknown}$	
R9	$O_2^* + O_2, N_2, O \xrightarrow{k_3^{O_2}, k_3^{N_2}, k_3^O} \text{prod.}$	$k_3^{O_2}, k_3^{N_2}, k_3^O - \text{unknown}$	
R10	$O_2^* \xrightarrow{A_3} O_2 + h\nu$	$A_3 - \text{unknown}$	

670

671 **Table 2.** Efficiencies  $\alpha$  of the different excited states of  $O_2$ .

$O_2(c^1\Sigma_u^-)$	$O_2(A'^3\Delta_u)$	$O_2(A^3\Sigma_u^+)$	$O_2(^5\Pi_g)$	Reference
0.03	0.12	0.04	0.66	Wraight (1982), Smith (1984)
0.04	0.18	0.06	0.5	Bates (1988)
0.03	0.18	0.06	0.52	López-González et al. (1992a, b, c)

672

673 **Table 3.** Fitting coefficients for combined mechanism (Eq. 5) at different efficiencies.

	Low $\tilde{\varepsilon}$ Wraight (1982)	High $\tilde{\varepsilon}$ Bates (1988)	Averaged $\tilde{\varepsilon}$ (this work)
$\tilde{\varepsilon}$	0.015	0.03	0.022
$D_1 = \tilde{k}_3^O / \tilde{k}_3^{O_2}$	$0.211^{+0.355}_{-0.136}$	$0.397^{+0.22}_{-0.282}$	$0.231^{+0.358}_{-0.142}$
$D_2 = \tilde{\alpha}\tilde{\gamma}$	$0.087^{+0.12}_{-0.041}$	$0.073^{+0.119}_{-0.042}$	$0.08^{+0.12}_{-0.04}$

674

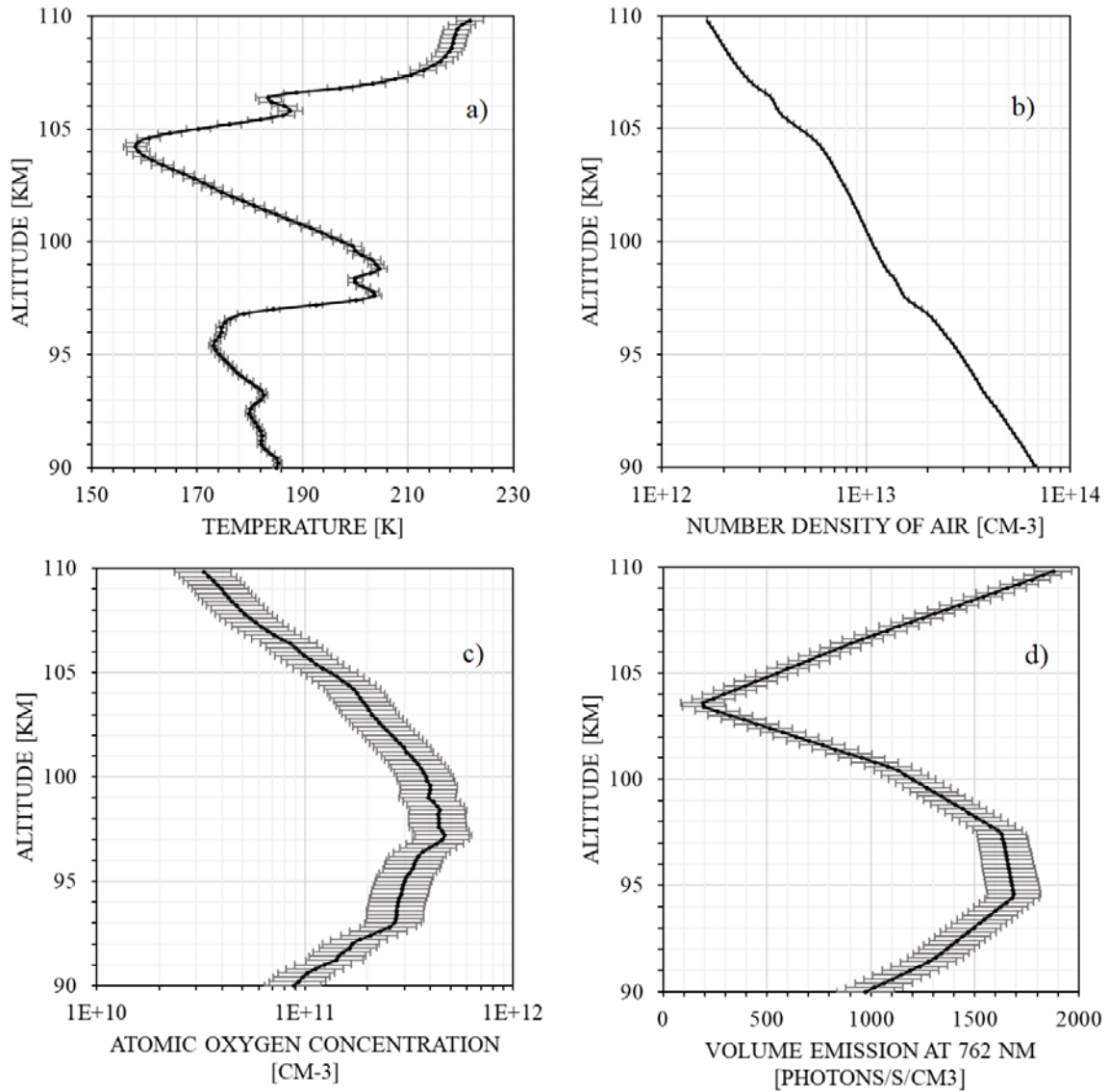
675

676

677 **Figures.**

678 Figure 1. Measurements of a) temperature (CONE), b) number density of air (CONE), c)

679 atomic oxygen concentration (FIPEX), d) volume emission at 762 nm (photometer).



680

681

682

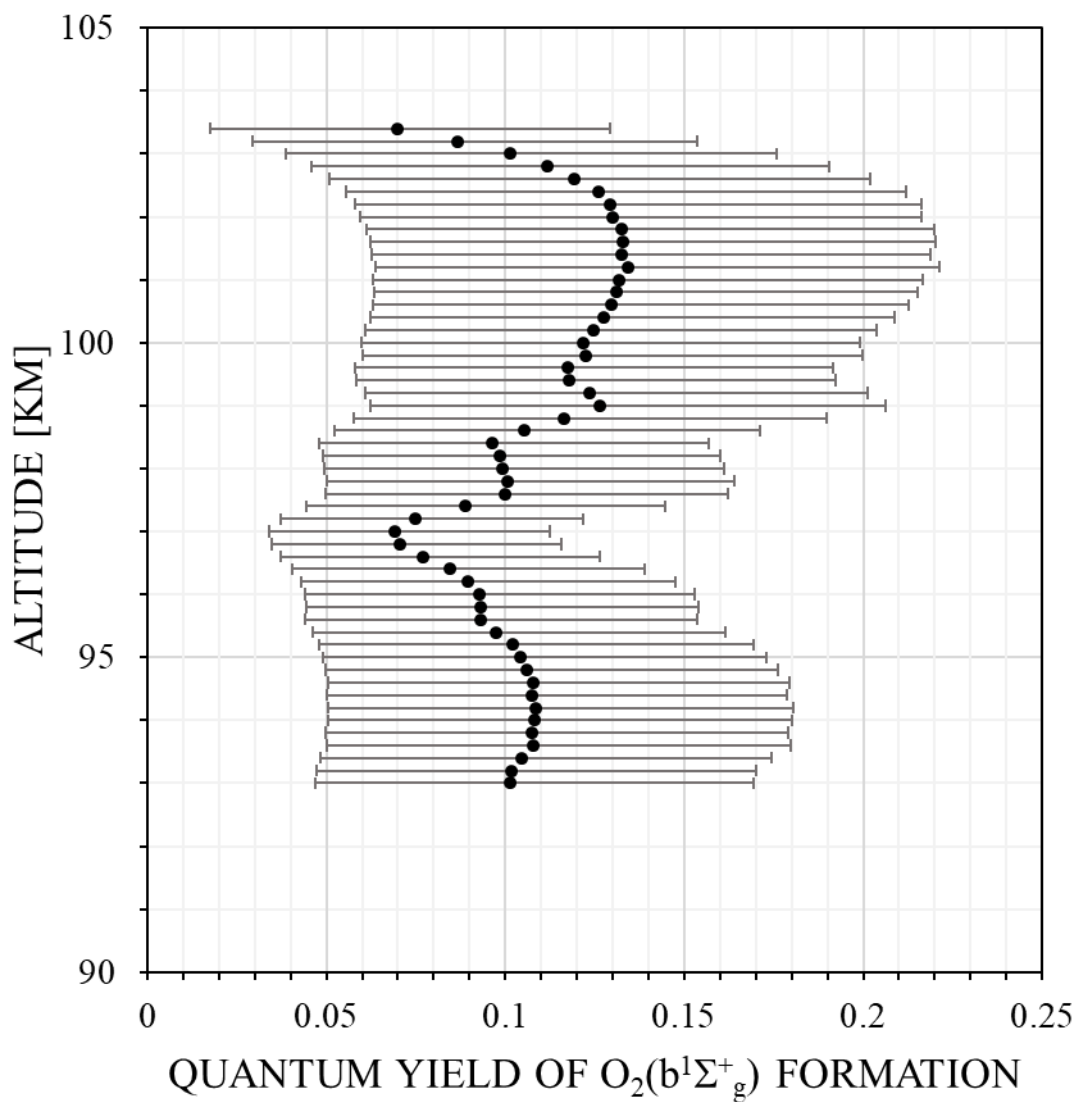
683

684

685

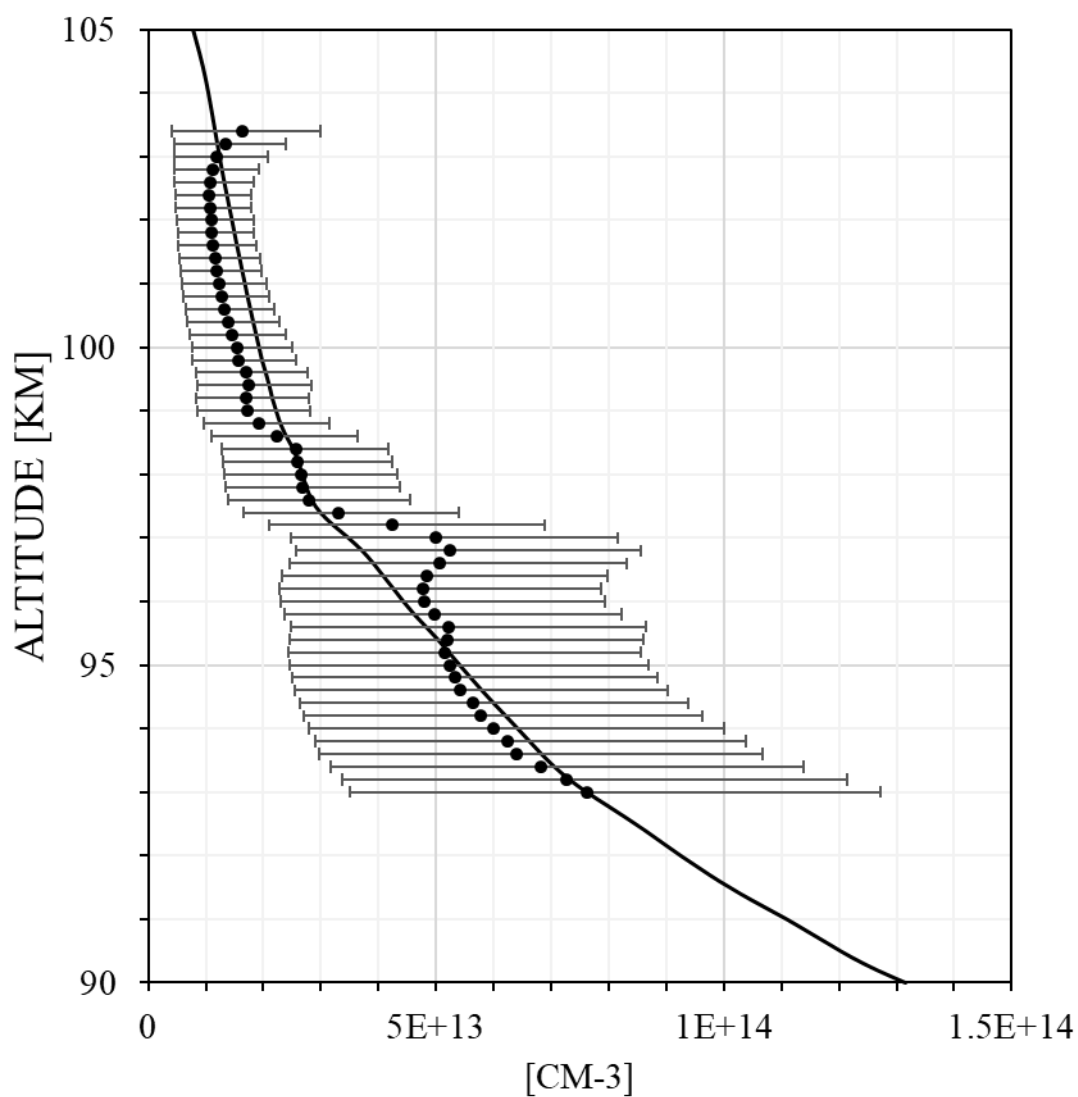
686

687 Figure 2. Quantum yield of  $O_2(b^1\Sigma_g^+)$  formation  $\varepsilon$  for the case of one-step mechanism.



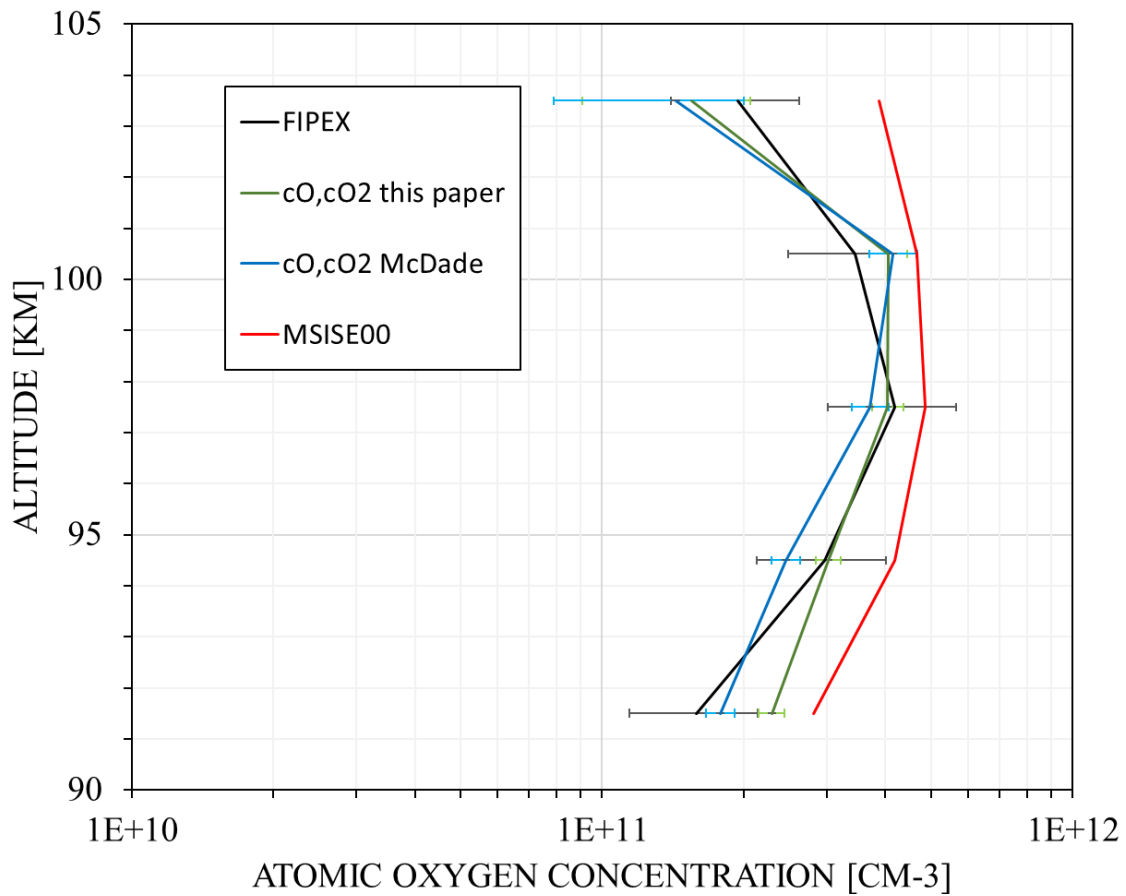
688  
689  
690  
691  
692  
693  
694  
695  
696  
697

698 Figure 3. RHS (dots) and least-square fit of LHS (black line) of equation (4).



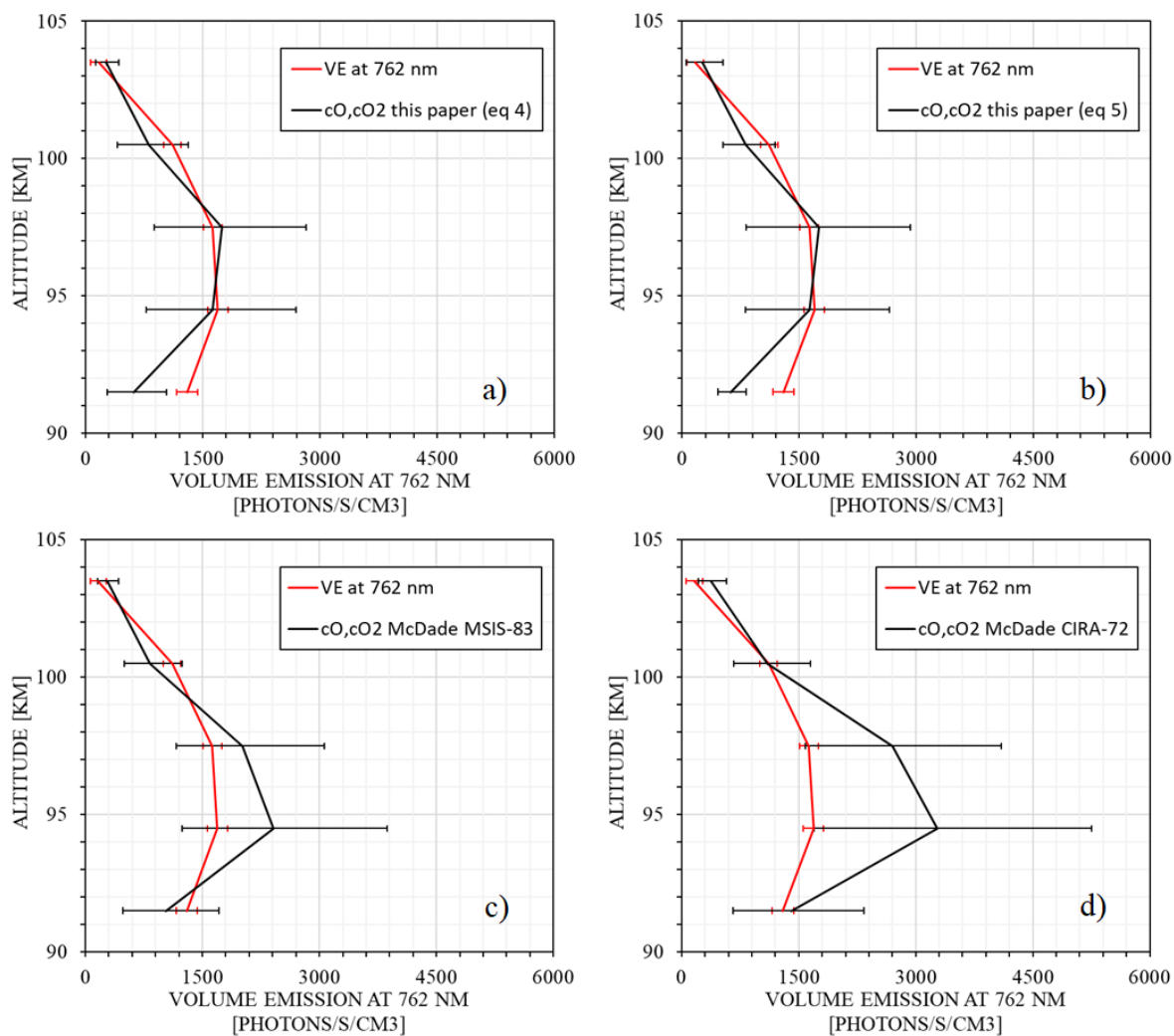
699  
700  
701  
702  
703  
704  
705  
706  
707  
708

709 Figure 4. Atomic oxygen concentration: FIPEX (black line); model MSISE00 (red line);  
710 derived from emission observation with McDade et al. (1986) coefficients (blue line);  
711 calculated with newly derived fitting coefficients for the two-step mechanism (green line).



712  
713  
714  
715  
716  
717  
718  
719  
720  
721  
722

723 Figure 5. Volume emissions: photometer (red line); derived from atomic oxygen (black line)  
 724 with a) newly derived fitting coefficients for the two-step mechanism, b) with fitting  
 725 coefficients for combined mechanism, c) with McDade et al. (1986) coefficients, which  
 726 correspond to the MSIS-83 temperature, and with McDade et al. (1986) coefficients, which  
 727 correspond to the CIRA-72 temperatures.



728